The International Society of Precision Agriculture presents the
15th International Conference on
Precision Agriculture
26–29 JUNE 2022
Minneapolis Marriott City Center | Minneapolis, Minnesota USA

Xiong Xiong[1]*, D. Brent Myers[1], Jason DeBruin[1], Bob Gunzenhauser[1], Naveen Sampath[1], Dening Ye[1], Haley Underwood[3], and Rebecca Hensley[4]

[1] Corteva Agriscience, 7000 NW 62nd Avenue, Johnston, Iowa 50131, USA; brent.myers@corteva.com(D.B.M.); jason.debruin@corteva.com (J.D.); naveen.sampath@corteva.com (N.S.); dening.ye@corteva.com (D.Y.); robert.gunzenhauser@corteva.com (R.G.)
[3] Corteva Agriscience, 21888 N 950th Road, Adair, Illinois 61455, USA; haley.underwood@corteva.com
[4] Corteva Agriscience, 3850 North 100 East, P.O. Box 26, Windfall, Indiana 46076, USA;rebecca.hensley@corteva.com
*Correspondence: xiong.xiong@corteva.com

Functional Soil Property Mapping with Electrical Conductivity, Spectral and Satellite Remote Sensors

Abstract.

Proximal electrical conductivity (EC) and spectral sensing has been widely used as a cost-effective tool for soil mapping at field scale. The traditional method of calibrating proximal sensors for functional soil property prediction (e.g., soil organic matter, sand, silt, and clay contents) requires the local soil sample data, which results in a field-specific calibration. In this large-scale study consisting of 126 fields, we found that the traditional local calibration method had suffered weak correlation or uninterpretable models due to confounding factors (e.g., soil moisture) and small field variability. We proposed a new global calibration method that integrates satellite remote sensing (i.e., SMAP soil moisture, Landsat 8, and MODIS) and topographic information to explicitly account for the confounding effects in a large domain for a more robust calibration. Results show that both global and local calibration showed marked reduction in total root mean squared error (RMSE) over SSURGO. Global calibration without local soil samples had comparable accuracy as the local calibration in predicting organic matter (OM), sand, silt, and clay at the depths of 0-30, 30-60, and 60-90 cm. Adding five local sample measurements to the global models (spiking) reduced the overall errors for all four soil attributes by correcting the cross-field errors resulting in the most accurate predictions. Our findings suggest that global calibration is a robust, accurate, and cost-effective solution for operational functional soil property mapping.

Keywords.
apparent electrical conductivity, spectroscopy, proximal sensing, remote sensing, soil organic matter, soil texture

Introduction

Precision agriculture technologies, such as variable-rate technology and crop-growth models require high-quality soil information as input (Corbeels et al., 2016; Jones et al., 2003; Maleki et al., 2008). While traditional soil survey maps can provide spatial soil information at landscape to regional scales, they often fall short to well represent the field-scale soil variability due to their small cartographic scales (Brevik et al., 2003; Stermitz et al., 1999). Soil sampling, on the other hand, can provide high-accuracy-precision and up-to-date soil information at point-scale, but the prohibitive cost associated with the field and laboratory work limits its scalability.

In the last two decades, proximal soil sensing technologies have been increasingly popular in soil mapping, among which electrical conductivity (EC) and spectroscopic sensors are commonly used (England and Viscarra Rossel, 2018; Kitchen et al., 2005; Myers et al., 2007; Viscarra Rossel et al., 2011). These proximal sensors capture georeferenced EC and spectral reflectance signals close or in contact with the soil *in situ*, which are then used to infer the functional soil properties through empirically calibrated models (Domsch and Giebel, 2004; Reyes et al., 2018; Rezaei et al., 2016; Serrano et al., 2014; Zare et al., 2021). Electrical conductivity of the bulk soil, also known as apparent EC or EC_a is affected by various soil properties, including soil texture, bulk density, cation exchange capacity (CEC), and soil moisture (Friedman, 2005; McCutcheon et al., 2006). *In-situ* soil spectral reflectance, e.g., red and near infrared band, is affected by soil organic matter (OM) content, soil moisture, and mineral composition, etc. (Angelopoulou et al., 2020; Bricklemyer and Brown, 2010; England and Viscarra Rossel, 2018). Because several factors can change the sensor signal, exploiting the correlation for functional soil property prediction is often confounded by the factors of lesser interest (Angelopoulou et al., 2020; McCutcheon et al., 2006). A common solution to this equifinality problem is calibrating the sensor data to some soil sample measurements in a confined domain, e.g., in a field, where the confounding effects are presumably small, resulting in a local calibration specific to the small domain (Yang et al., 2022).

A major problem with the local calibration approach without explicitly accounting for the confounding effects is that a successful calibration is not guaranteed for every field because some fields may display weak or even no correlation between sensor data with the soil sample measurements. One solution to address this issue is to expand the calibration domain, e.g., to multiple fields at regional scale, with sufficiently large soil sample size and soil covariate data from remote sensors to account for the confounding effects. Another benefit of the large-domain global calibration is that it eliminates the need for local soil sample data for functional soil property predictions. In the case where local soil samples are available, global model calibration can incorporate the local data in the recalibration, i.e., model spiking, for improved local prediction accuracy. This technique has proved effective by many studies that use laboratory near-infrared spectroscopy in soil property prediction including soil organic carbon, total nitrogen, sand, silt, clay, pH, and phosphorus (Jiang et al., 2017; Kuang and Mouazen, 2013).

In this study, a global calibration approach that integrates proximal EC, spectral, and remote sensing data from multiple fields was proposed. The objectives of this study were to 1) understand the variability of the field-specific relationships between proximal sensor data (EC_a, NIR, and red) and functional soil properties (OM, sand, silt, and clay), 2) investigate the effectiveness of the large-domain global calibration compared with the local calibration approach in the accuracy of functional soil property predictions, and 3) how the spiking of global calibration with local samples affects the accuracy of the global models.

Materials and Methods

Field Data Collection and Laboratory Analysis

This large-scale study consists of field soil and sensor data collected from a total of 126 fields across the Corn Belt in the USA from 2016 to 2019. A typical field workflow started with a Veris® sensor survey. After the data had passed the quality checked by Veris, the EC_a deep channel data was used to guide the soil sampling of 5 to 15 locations in the field such that the full range of EC_a was well represented. Soil samples were taken at three depths, i.e., 0-30, 30-60, and 60-90 cm, and then sent to Waypoint Analytical™ for OM and texture test. Within 1 m of the soil sample cores, additional cores were pulled for gravimetric soil moisture and bulk density measurement.

Fig. 1. Veris survey and field sampling locations of 126 fields in the United States.

Proximal Soil Sensors

Veris model used in this study was V3210 (Veris Technologies, Salina, Kansas) equipped with an EC_a and an OpticMapper sensor. The EC_a sensor had a dual-channel array that responds to signals from shallow (0-30 cm) and deep (0-90 cm) depths. A simple average of the two channels was calculated to represent a mid-depth (0-60 cm). The OpticMapper sensor collected red and near-infrared reflectance through a sapphire window on the bottom of a furrow 'shoe' that cut in the surface soil at 2.5-7.6 cm depth.

Soil Covariates

Various spatio-temporal soil covariates were collected to characterize the field condition when field data collection occurred.

Table 1. Summary of covariates

Data Category	Resolution/Scale	Covariates
SMAP	9 km	surface, rootzone soil moisture
Landsat 8	30 m	blue, green, red, NIR, SWIR, TIRS, BSI
MODIS	250 m - 1 km	blue, green, red, NIR, BSI, SWIR
DTA	10 m	elevation, slope, curvature, channel distance, TPI, SWI
SSURGO	1:24,000	organic matter, sand, silt, clay

SMAP Soil Moisture

SMAP L4 surface and root zone soil moisture analysis update data provides global volumetric soil moisture at 9 km spatial resolution and 3-hour frequency (Reichle et al., 2019). The 3-hourly SMAP data of the same Veris survey date was temporally averaged to get daily soil moisture.

Digital Terrian Attributes

USGS National Elevation Dataset (10 m resolution) from USGS was used to derive digital terrain attributes (DTA) (Gesch et al., 2018). Smoothed elevation, slope, curvature, topographic position index (TPI), channel distance, and SAGA wetness index (SWI) were generated with SAGA GIS

(Conrad et al., 2015).

Long-term Bare Soil Imagery Composite

Large-scale bare soil imagery composites from 2014 to 2018 were generated for multiple satellite data sources: Landsat 8 Surface Reflectance (SR), Landsat 8 Top of Atmosphere (TOA) Brightness Temperature, and MODIS daily products (i.e., MOD09GQ, MOD09GA and MODTBGA). The raw satellite data was obtained for each available day in the period of 120 days prior to the county-level planting dates surveyed by USDA annually, and the obscuration (e.g., cloud, shadow, snow, waterbody) in the raw data were masked out by using the corresponding pixel quality bands. The Bare Soil Index (BSI) was computed pixel-wise to filter out the non-bare-soil pixels as in Eq. (1). The resultant bare soil images were then temporally averaged to form the 2014-2018 composites with reduced temporal noises from soil moisture, crop residue, etc.

$$BSI = \frac{(SWIR + Red) - (NIR + Blue)}{(SWIR + Red) + (NIR + Blue)} \quad (1)$$

Data Analysis

For covariates with the depth dimension, i.e., SSURGO and SMAP data, they are resampled to the sample depth interval as the soil samples using depth-weighted average. Then all the covariates were joined to the soil sample data with longitude, latitude, and depth as the composite primary key. Finally, for the proximal sensor data, five nearest sensor readings to a soil sample location were averaged and joined to form a complete dataset for analysis.

Feature Selection

The Boruta all-relevant variable selection method was applied to identify the covariates that are strongly or weakly relevant to the functional soil properties, i.e., OM, sand, silt, and clay (Kursa and Rudnicki, 2010).

Data Split

The 126 fields were randomly split into three groups: training (70%) for model fitting, validation (15%) for hyper-parameter tuning in global calibration, and test (15%). In the test subset, there are 10 fields that have more than 10 soil profiles sampled, which were the data for local calibration and test of all models.

Local calibration

Local calibration was applied to the 10 test fields with more than 10 soil profiles sampled. Five samples corresponding to the min, 25th percentile, 50th percentile, 75th percentile, and max of EC_a deep channel and NIR for texture and OM models, respectively, were selected for depth-wise calibration using Ordinary Least Squared linear model as in Eq. 2 and 3. Then the remaining samples in the same field were used for local calibration model test.

$$Sand_{depth},\ Silt_{depth},\ or\ Clay_{depth} = a + b \cdot EC_{DP} + \varepsilon \quad (2)$$

where, Sand, Silt, or Clay is the laboratory measured texture fraction content in % mass, depth is soil layer depth (i.e., 0-30, 30-60, 60-90 cm), a is the intercept, b is slope, EC_{DP} is the EC_a deep channel, and ε is the random error.

$$OM_{depth} = a + b \cdot NIR + \varepsilon \quad (3)$$

where, OM is the laboratory measured OM in % mass, depth is soil layer depth (i.e., 0-30, 30-60, 60-90cm), a is the intercept, b is slope, NIR is the NIR band, and ε is the random error.

Global calibration and spiking

In the global calibration, all fields from the training subset were pooled and used to fit global

XGBoost regression models for OM, sand, silt, and clay at 0-30, 30-60, and 60-90 cm depths, respectively. For spiking, the five local calibration samples from each of the 10 test fields were added to the training set of the global calibration training set and the global calibration models were refitted with the expanded training set. Both global calibration and spiked global calibrations models were tested against the same set of test samples as in the local calibration to ensure a fair comparison of all three models.

Error Partitioning

The MSE is decomposed into within-field and cross-field MSE, and then each of the terms was reported in the RMSE. The cross-field RMSE is to quantify the bias in the field mean estimation and within-field RMSE is to assess the precision in explaining the within-field soil variability.

$$MSE_{total} = MSE_{cross\_field} + MSE_{within\_field} \quad (4)$$

Model Interpretation

SHAP values represent a feature's responsibility contribution for a change in the model output (Lundberg and Lee, 2017). The feature importance is summarized as the absolute mean SHAP values over the training data.

Results

Table 2. Field-level descriptive statistics of measured soil properties

	Depth	Field mean							Field standard deviation			
	(cm)	Mean	SD	Min	25%	50%	75%	Max	Mean	25%	50%	75%
OM	0-30	3.02	1.06	0.75	2.31	3.0	3.72	5.8	0.48	0.29	0.41	0.62
(%)	30-60	2.06	0.62	0.52	1.64	2.1	2.5	3.9	0.37	0.24	0.32	0.47
	60-90	1.57	0.49	0.43	1.23	1.57	1.94	3.17	0.31	0.18	0.26	0.39
Sand	0-30	34	18	16	22	29	43	93	5	3	4	6
(%)	30-60	36	17	16	22	31	42	93	6	3	6	9
	60-90	37	21	15	20	29	47	93	6	2	5	9
Silt	0-30	48	16	4	40	52	60	75	4	3	4	5
(%)	30-60	45	15	4	36	50	57	70	6	3	5	7
	60-90	44	18	4	32	50	59	67	5	3	4	7
Clay	0-30	18	6	3	14	17	21	37	3	2	2	3
(%)	30-60	19	6	3	15	19	22	40	3	2	3	4
	60-90	19	7	3	15	19	23	40	3	2	3	5
ECsh		38	18	4	26	39	50	85	7	3	6	9
EC_{dp}		42	19	4	30	44	54	90	6	3	6	8
Red		159	25	60	149	158	166	323	4	2	2	4
NIR		451	34	346	434	449	467	570	12	4	7	15

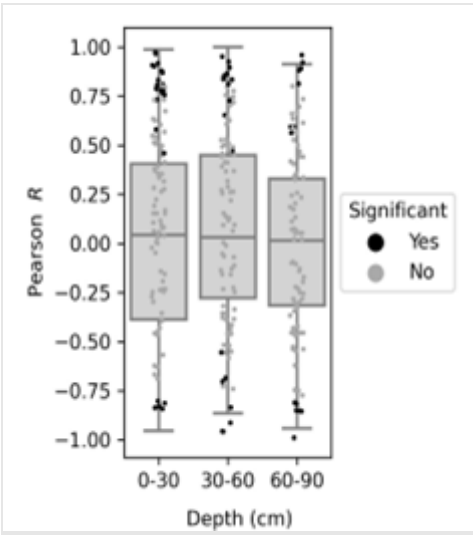

Fig. 2. Pearson's correlation between soil moisture and clay content by field statistically tested at 0.9 confidence level

Local Calibration

Measured clay content and EC_a channels had positive Pearson's correlation in more than half of the fields at 0-30 and 30-60 cm depths for both shallow and deep channels, while the correlation was weaker in the 60-90 cm layer with a near zero median correlation coefficient as shown in **Fig. 3** (a) and (b). The correlation coefficients also showed large variance across fields ranging from -0.99 to 0.97. In the statistical test, the correlation was significant at 90% confidence level for only about 13% of 126 fields across the three layers and five of these fields had significantly negative correlation. **Fig. 4** (a) and (b) showed that although the mean clay content was not different between the group with significant clay-EC correlation and the one not, the within-field variance of clay had marked difference between the two groups. This indicates that within-field variability of the soil texture is a differentiator of the significance of clay-EC correlation, meaning that it is more likely to find significant correlation in fields with greater texture variability. Measured OM was mostly negatively correlated with NIR and red bands, with a correlation strength generally decreasing along the soil profile as seen in **Fig. 3**(c) and (d). Large variance in OM-red/NIR correlation coefficient was observed across fields ranging from -0.99 to 0.99 with about 15 % of the fields had the correlation tested significantly at 90 % confidence level. Similarly, the within-field variance of OM was a differentiator of whether the OM-red/NIR correlation was significant, even though not as strong in the case of clay-EC.

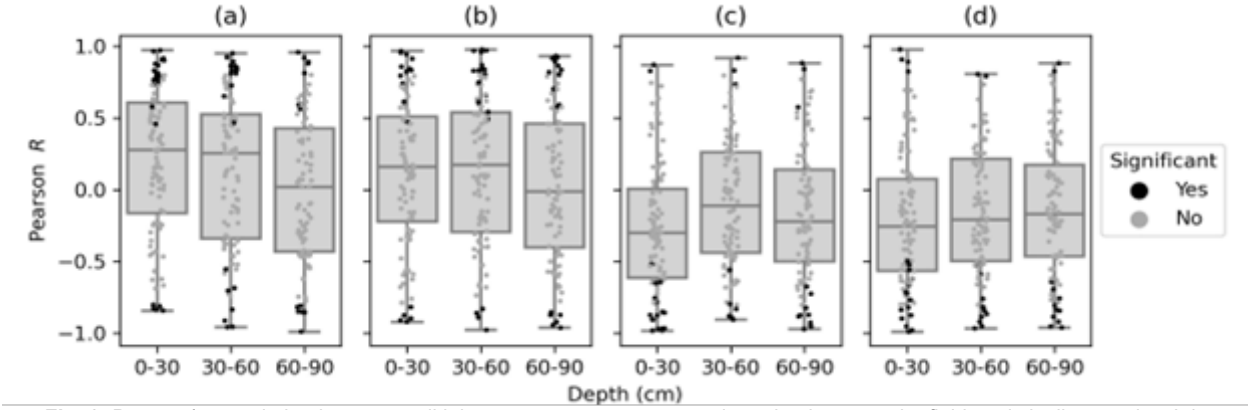

Fig. 3. Pearson's correlation between soil laboratory measurements and proximal sensors by field statistically tested at 0.9 confidence level: (a) clay content (%) and EC_a shallow channel; (b) clay content (%) and EC_a deep channel; (c) OM content (%) and red; (d) OM content (%) and near infrared

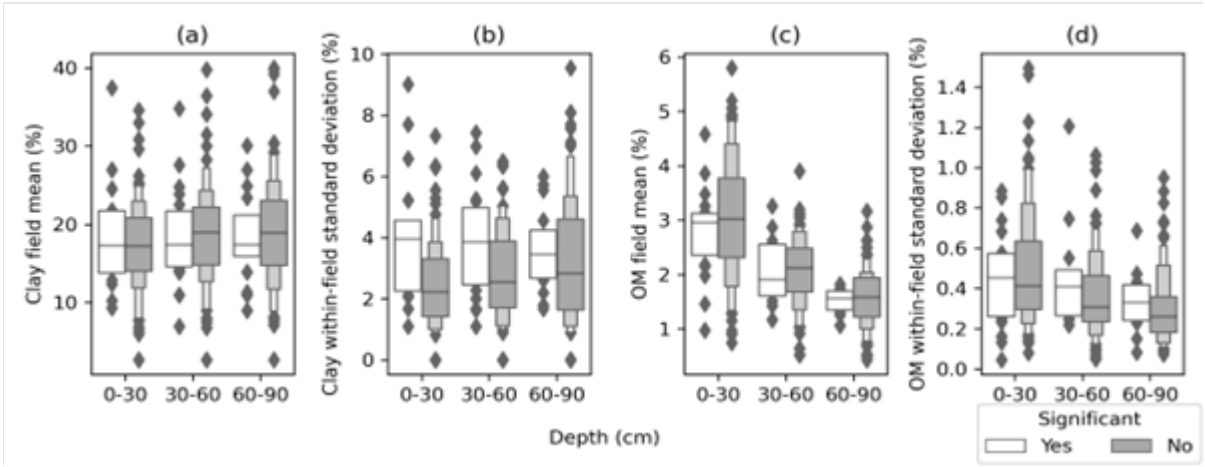

Fig. 4. Mean and standard deviation of soil measurements by field: (a) clay content (%) and EC_a shallow channel; (b) clay content (%) and EC_a deep channel; (c) OM content (%) and red; (d) OM content *(%) and near infrared.*

The validation of local calibration model predictions against measured OM, sand, silt and clay content from the independent test dataset showed an overall success across fields with low biases (**Fig. 5**) in texture properties and marked total RMSE reduction compared with the publicly available SSURGO data (**Fig. 6**). This large accuracy improvement came primarily from the cross-

field error reduction, indicating the local training data had provided improved estimation of the field means of all the soil attributes. Although in some of the fields, local calibration did not predict the test sample data well, e.g., the red color field as shown in **Fig. 5**, the overall within-field error reduction across all fields and depths was marked, ranging from about 20 to 45 % lower RMSE compared with SSURGO.

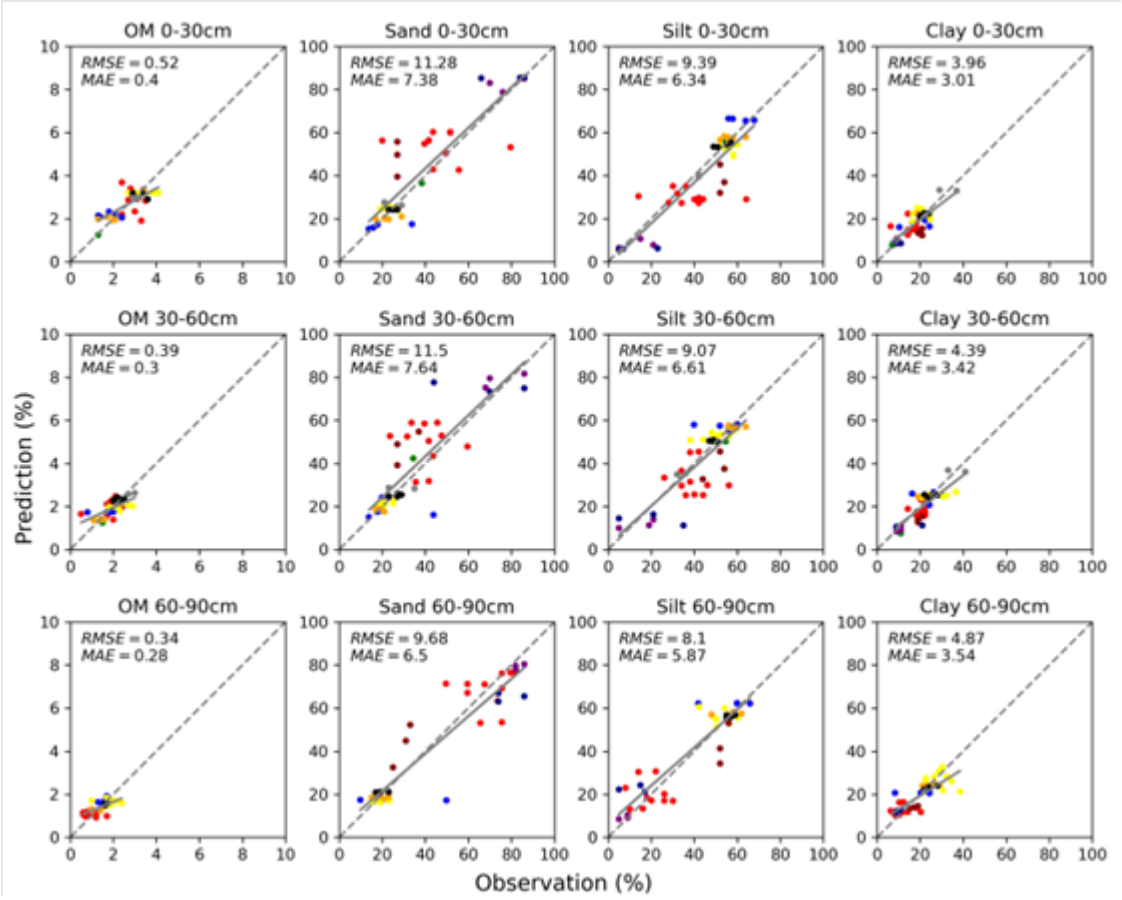

Fig. 5. Independent validation for local calibration color grouped by fields

Global calibration and spiking

Global calibration models without any local samples achieved the same level of within-field RMSE as the local calibration, indicating model learning from other fields can be applied to new fields. The global calibration generally performed worse in capturing the field level variability compared with the local calibrations as seen in the higher cross-field RMSE in **Fig. 6**, which consequently resulted in a higher total RMSE. However, global calibration had much improved error compared with SSURGO and was more cost-effective than the local calibration.

When spiked with local samples, the global calibration models had similar or better cross-field and total RMSE compared with the local calibration (**Fig. 6**), showing that local samples were useful to correct the bias in the field means. However, local samples did not help with within-field error reduction and did not show any sign of overfitting either.

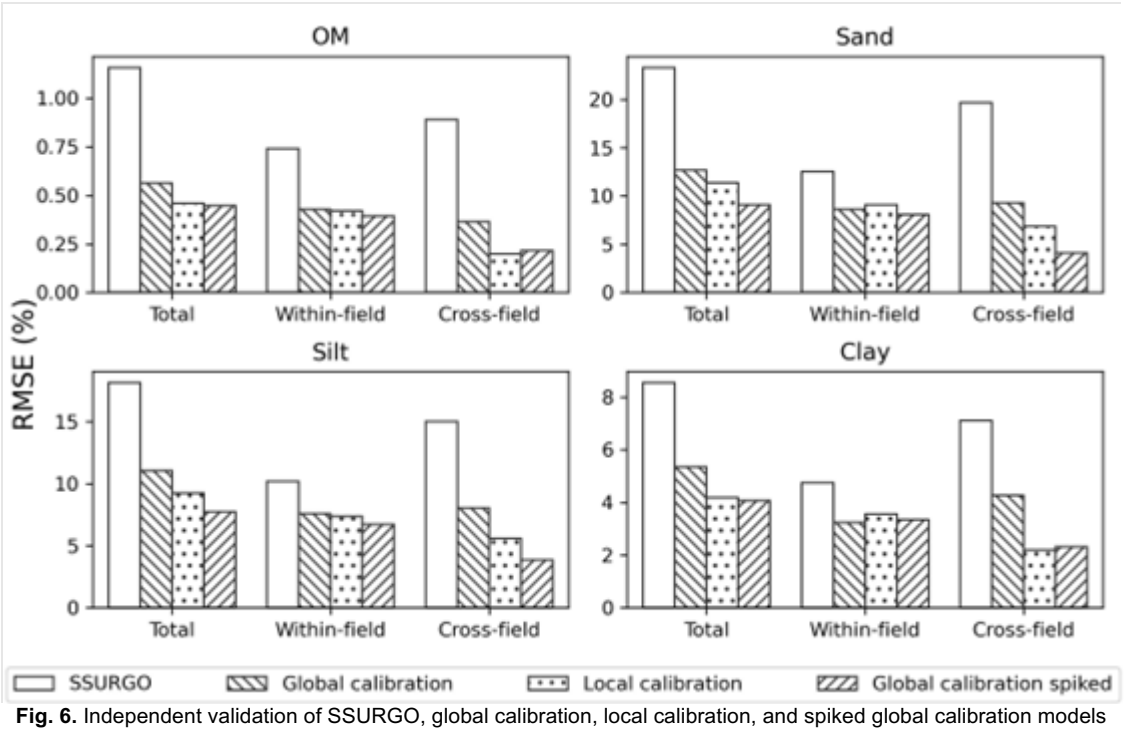

Fig. 6. Independent validation of SSURGO, global calibration, local calibration, and spiked global calibration models

The interpretation of the non-linear tree-based global calibration models was shown in the variable importance that is measured in the mean absolute SHAP values (**Fig. 7**). Generally, the predictors with large-scale effects were most important, e.g., SSURGO, MODIS, SMAP, followed by the fine-scale proximal sensor data. The reason is that the cross-field variance was much greater than the within-field variance dominant component in the total variance in the measured soil data (**Table 2**), so those variables that explained the cross-field variance dominated the models, which can be confirmed with the RMSE components in **Fig. 6**. The SMAP soil moisture ranked high in the clay model, suggesting the moisture effect was effectively adjusted by the satellite soil moisture data in the global calibration.

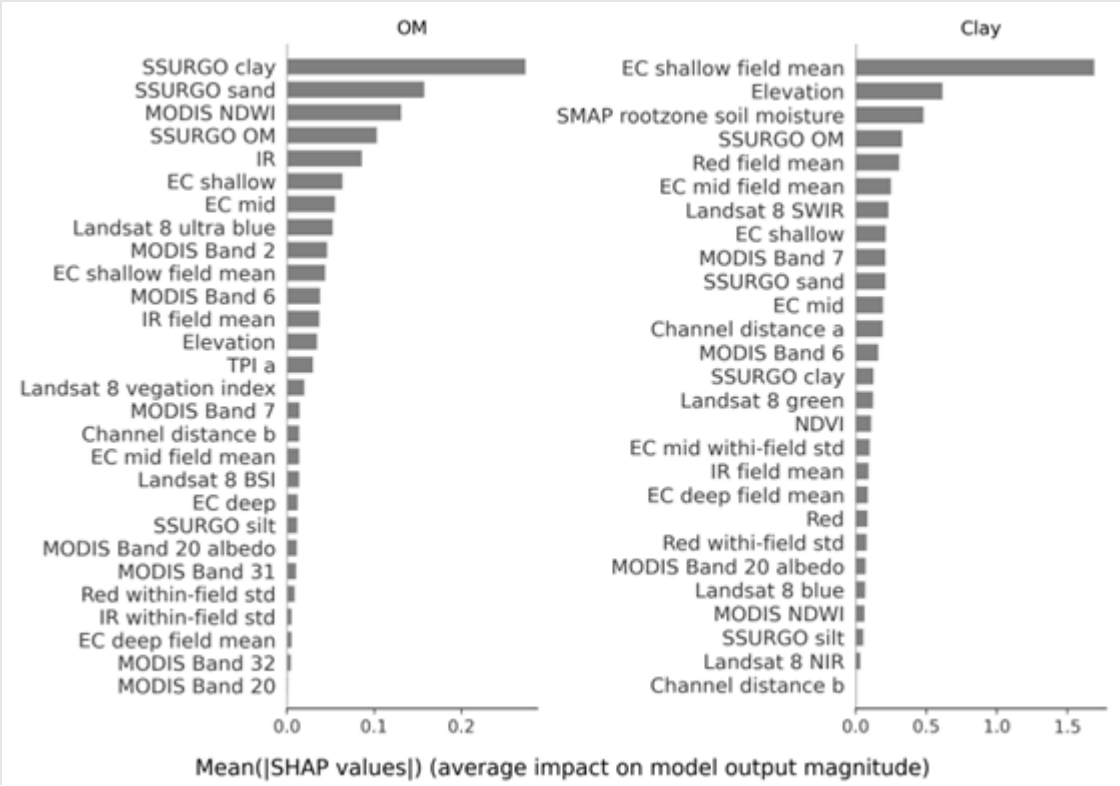

Fig. 7. Variable importance in global calibration models

Discussion

To the best of our knowledge, this is the first large-scale study examining and validating different calibration methods for functional soil mapping with proximal EC and optical sensors. The diversity in soil types, land management, and topography across the 126 corn/soybean growing fields in the United States allows for vigorous test of the feasibility, generalizability, and robustness of using the proximal EC_a and spectroscopic sensors to map functional soil properties.

The power and limitations of local calibration

Proximal sensors allow rapid, continuous field measurement of apparent soil conductivity and spectroscopic reflectance, but its comparability and generalizability across fields are commonly questioned due to field-specific and dynamic factors that can shift and stretch the distributions of sensor readings. Therefore, mapping of EC_a and spectroscopic data into functional soil properties such as OM, texture is done through field-specific calibration to a few local soil samples with a linear regression model, which presumably avoids the need to tease out the main effects among the confounding factors to accurately predict the target functional soil attributes.

From the result of the 126 fields, we found that the success of local calibration varied. Less than 20 % of the fields exhibited statistically significant correlation between OM, texture and Red/NIR, EC_a, respectively (**Fig. 3**). The independent test of local calibration models in the 10 fields also showed inconsistent correlation between predictions and observations when examined on a field basis (**Fig. 5**). There are at least three factors that are pertinent to this mixed result: the within-field inherent soil variability, the spatial correlation between the main and confounding factors, and the interaction effects between the main and nuance factors. These three factors can be conceptually expressed in a linear model as in Eq. 5:

$$EC_a = a + b \cdot Clay + c \cdot Moisture + d \cdot Clay \cdot Moisture + \varepsilon \quad (5)$$

where, a is the intercept, *b·Clay* is the effect of the main factor clay, *c·Moisture* is the confounding effect from soil moisture, *d·Clay·Moisture* is the interaction effect of clay and soil moisture, and ε is the error term.

However, a typical local calibration only includes the main effect term without accounting for the moisture and the interaction effects due to the limited sample size. This leaves the model susceptible to the nuance factor and the interaction effects. In fields where the spatial correlation between clay and moisture is strong that can be explained by a linear model:

$$Moisture = a_m + m \cdot Clay + \varepsilon_m \quad (6)$$

where, am is the intercept, m·Clay is the effect from clay on soil moisture, and ε_m is the random error. If there is negligible interaction between clay and moisture, then Eq. 5 can be reduced to:

$$EC_a = a_n + b_n \cdot Clay + \varepsilon_n \quad (7)$$

where, a_n=a+a_m, b_n=b+b_m and ε_n=ε+ε_m

Then it is more likely to have reliable local calibration. On the other hand, if there is weak linear correlation between the main and nuance factors or strong interaction between them, the statistical significance of local calibration is compromised.

Clay and soil moisture are known to have spatial correlation because they are usually associated in the depositional geomorphological process and affected by topography. In a catena, footslopes and toeslopes tend to accumulate soil water and depositional clay from higher slopes. In addition, soils with more clay content to a certain level usually have greater permanent wilting point and field capacity. In this study, most of the fields exhibited this positive correlation in all three depths as in **Fig. 2**. However, the strength of the clay-moisture correlation varied markedly, and some fields even showed significant negative correlation, which may weaken or cancel out the effect of clay on EC_a.

The third factor worth noting is signal-noise ratio pertinent to the true soil variability over the laboratory measurement and field sensor errors. From **Fig. 4**, the strong significant correlation tends to be found in fields where within-field variability was large. In the fields with small variability, the main effects from the OM or texture can be masked by the random error ε. From this study, the median within-field standard deviation of the fields that had significant correlation for clay and OM were about 4 % and 0.4 %. These findings provide the first the sensitivity of the proximal sensor in mapping functional soil attributes.

Global calibration

The goal of global calibration by leveraging a much larger pooled dataset to address the issues of local calibration, reduce the operational cost, and improve scalability of this soil mapping tool.

One immediate benefit of the large sample size is that it opens the door to more expressive machine learning models that allow for more parameters to account for the confounding effects and represent the non-linear effects in the main factors. In addition, more covariates such as the satellite sensor data from Landsat 8, MODIS, and SMAP, can be integrated to explain the large-scale cross-field soil variability and account for the confounding effects such as soil moisture. The validation in this study in the 10 independent test fields demonstrates that this approach without the need to collect any local soil samples can effectively explain both cross-field and within-field soil variability with marked improvement over SSURGO. When compared with local calibration, global calibration can have similar precision as indicated by the within-field errors. In terms of bias of the field means as benchmarked by the local calibration, global calibration indeed showed greater errors, suggesting there was still some cross-field soil variability that is not explainable with the remote sensing, DTA, and SSURGO predictors. Further exploration of new cross-field covariates in correcting the field-mean bias is suggested.

Spiking the global model with local samples shows success in correcting the biases in field means for all soil attributes. This technique was first introduced by (Kuang and Mouazen, 2013) in their research in using laboratory near-infrared spectroscopy for within-field soil characterization and shown to considerably improve the RMSE from the global model trained with a national library of soil spectroscopy. Since then, it has been reported in many studies in spectroscopic modeling to successfully improve local prediction accuracy for various soil attributes including soil organic carbon, total nitrogen, sand, silt, clay, pH, and phosphorus (Jiang et al., 2017). This study shows that spiking the global calibration model produces the most accurate predictions of OM, sand, silt, and clay among all model approaches and proves its effectiveness in much broader environments than previous ones. With the error decomposition, this study is the first to show that the source of improvement mainly comes from the correction of biases in the field means due to the local samples, followed by moderate improvement in explaining the within-field soil variability.

Applications in precision agriculture and carbon accounting

While EC_a has been used in management zone delineation, functional soil maps are required by decision support tools such as crop growth model for farmers to make precise decisions in nitrogen, fertility, and water management (Bobryk et al., 2016). The accuracy of input soil data has a profound impact on the quality of the decisions. (Varella et al., 2010) conducted a global sensitivity analysis on wheat crop model with respect to soil parameters and found a significant relation between the global quality of the estimation of seven soil parameters including OM and texture. In a global sensitivity analysis on maize crop models, (Corbeels et al., 2016) found the genetic coefficients, the mineral nitrogen fertilization, and the organic carbon of the first soil layer were the most determining factors for the simulated crop production variables. In our internal local sensitivity analysis on DDSAT maize crop growth model, 1 % RMSE from the OM parameter in the first layer can lead to 22 kg ha^{-1} total nitrogen simulation error. These studies suggest that given the level of errors in the publicly available SSURGO data as shown in **Fig. 6** (i.e., 0.75-1.2 % RMSE in OM, and 7-26 % in sand, silt, and clay), it is advisable to take note of the errors that could be induced by the quality of the soil input when using these decision support tools in precision agriculture.

The other key factor worth noting is the operating cost of the proximal soil sensing tool. Proximal sensing has been acclaimed to be a rapid and cost-effective way to map soil EC_a. In this study, we have proposed and tested the global calibration method integrated with satellite sensors as an effective way to map the EC_a data into functional soil properties. It is encouraging to find that global calibration without the requirement to collect local calibration soil samples can achieve comparable accuracy explaining the within-field variability that matters most to the precision agriculture application.

The other promising application that requires accurate soil data is the soil carbon quantification to enable the soil carbon sequestration market. Current field proximal sensing based approach relies solely on the field VNIR spectroscopy (Jiang et al., 2017). In this study, we found the EC_a can also be used along with spectroscopic sensors in SOC quantification as indicated by **Fig. 7**. In the soil carbon quantification, the low field-mean bias is the primary objective function to optimize for. We proved that spiking of the global calibration model with as few as five local samples can achieve 0.25 % OM field mean RMSE in 0-90 cm soil profile, which suggests that this approach is sensitive to detect the OM change as low as 0.5 % at field scale. To completely remove the local calibration sample requirement, further research in correcting the biases in field means with scalable satellite sensor data is warranted.

Conclusions

- Although local calibration is used as a common practice in mapping proximal EC_a and spectroscopy sensor data into functional soil properties, the quality of the result varies and is

highly susceptible to field-specific conditions, e.g., confounding factors, interactions, and meaningful inherent within-field soil variability.

- Global calibration integrating satellite sensor data without local calibration samples provides a more cost-effective solution than local calibration for functional soil property mapping with a comparable within-field error.
- Spiked global calibration produces the most accurate models by correcting the cross-field errors.
- The proposed methods have great potential to be used in precision agriculture and soil carbon quantification thanks to the high accuracy and reduced cost in quantifying functional soil properties.

References

Angelopoulou, T., Balafoutis, A., Zalidis, G., Bochtis, D., 2020. From laboratory to proximal sensing spectroscopy for soil organic carbon estimation: A review. Sustainability 12, 443. https://doi.org/10.3390/su12020443

Bobryk, C.W., Myers, D.B., Kitchen, N.R., Shanahan, J.F., Sudduth, K.A., Drummond, S.T., Gunzenhauser, B., Raboteaux, N.N.G., 2016. Validating a digital soil map with corn yield data for precision agriculture decision support. Agronomy Journal 108, 957–965. https://doi.org/10.2134/agronj2015.0381

Brevik, E.C., Fenton, T.E., Jaynes, D.B., 2003. Evaluation of the accuracy of a Central Iowa soil survey and implications for precision soil management. Precision Agriculture 4, 331–342. https://doi.org/10.1023/A:1024960708561

Bricklemyer, R.S., Brown, D.J., 2010. On-the-go VisNIR: Potential and limitations for mapping soil clay and organic carbon. Computers and Electronics in Agriculture 70, 209–216. https://doi.org/10.1016/j.compag.2009.10.006

Conrad, O., Bechtel, B., Bock, M., Dietrich, H., Fischer, E., Gerlitz, L., Wehberg, J., Wichmann, V., Böhner, J., 2015. System for automated geoscientific analyses (SAGA) v. 2.1.4. Geoscientific Model Development 8, 1991–2007. https://doi.org/10.5194/gmd-8-1991-2015

Corbeels, M., Chirat, G., Messad, S., Thierfelder, C., 2016. Performance and sensitivity of the DSSAT crop growth model in simulating maize yield under conservation agriculture. European Journal of Agronomy 76, 41–53. https://doi.org/10.1016/j.eja.2016.02.001

Domsch, H., Giebel, A., 2004. Estimation of soil textural features from soil electrical conductivity recorded using the EM38. Precision Agriculture 5, 389–409. https://doi.org/10.1023/B:PRAG.0000040807.18932.80

England, J.R., Viscarra Rossel, R.A., 2018. Proximal sensing for soil carbon accounting. SOIL 4, 101–122. https://doi.org/10.5194/soil-4-101-2018

Friedman, S.P., 2005. Soil properties influencing apparent electrical conductivity: a review. Computers and Electronics in Agriculture, Applications of Apparent Soil Electrical Conductivity in Precision Agriculture 46, 45–70. https://doi.org/10.1016/j.compag.2004.11.001

Gesch, D.B., Evans, G.A., Oimoen, M.J., Arundel, S., 2018. The National Elevation Dataset. American Society for Photogrammetry and Remote Sensing, pp. 83–110.

Jiang, Q., Li, Q., Wang, X., Wu, Y., Yang, X., Liu, F., 2017. Estimation of soil organic carbon and total nitrogen in different soil layers using VNIR spectroscopy: Effects of spiking on model applicability. Geoderma 293, 54–63. https://doi.org/10.1016/j.geoderma.2017.01.030

Jones, J.W., Hoogenboom, G., Porter, C.H., Boote, K.J., Batchelor, W.D., Hunt, L.A., Wilkens, P.W., Singh, U., Gijsman, A.J., Ritchie, J.T., 2003. The DSSAT cropping system model. European Journal of Agronomy 18, 235–265. https://doi.org/10.1016/S1161-0301(02)00107-7

Kitchen, N.R., Sudduth, K.A., Myers, D.B., Drummond, S.T., Hong, S.Y., 2005. Delineating productivity zones on claypan soil fields using apparent soil electrical conductivity.

Computers and Electronics in Agriculture 46, 285–308. https://doi.org/10.1016/j.compag.2004.11.012

Kuang, B., Mouazen, A.M., 2013. Effect of spiking strategy and ratio on calibration of on-line visible and near infrared soil sensor for measurement in European farms. Soil and Tillage Research 128, 125–136. https://doi.org/10.1016/j.still.2012.11.006

Kursa, M.B., Rudnicki, W.R., 2010. Feature selection with the Boruta Package. J. Stat. Softw. 36, 1–13.

Lundberg, S.M., Lee, S.-I., 2017. A unified approach to interpreting model predictions, in: Advances in Neural Information Processing Systems. Curran Associates, Inc.

Maleki, M.R., Mouazen, A.M., De Ketelaere, B., Ramon, H., De Baerdemaeker, J., 2008. On-the-go variable-rate phosphorus fertilisation based on a visible and near-infrared soil sensor. Biosystems Engineering 99, 35–46. https://doi.org/10.1016/j.biosystemseng.2007.09.007

McCutcheon, M.C., Farahani, H.J., Stednick, J.D., Buchleiter, G.W., Green, T.R., 2006. Effect of soil water on apparent soil electrical conductivity and texture relationships in a dryland field. Biosystems Engineering 94, 19–32. https://doi.org/10.1016/j.biosystemseng.2006.01.002

Myers, D.B., Kitchen, N.R., Sudduth, K.A., Sharp, R.E., Miles, R.J., 2007. Soybean root distribution related to claypan soil properties and apparent soil electrical conductivity. Crop Science 47, 1498–1509.

Reichle, R., De Lannoy, G., Koster, R.D., Crow, W.T., Kimball, J.S., Liu, Q., 2019. SMAP L4 global 3-hourly 9 km EASE-Grid surface and root zone soil moisture analysis update, Version 4. NASA National Snow and Ice Data Center Distributed Active Archive Center.

Reyes, J., Wendroth, O., Matocha, C., Zhu, J., Ren, W., Karathanasis, A. d., 2018. Reliably mapping clay content coregionalized with electrical conductivity. Soil Science Society of America Journal 82, 578–592. https://doi.org/10.2136/sssaj2017.09.0327

Rezaei, M., Saey, T., Seuntjens, P., Joris, I., Boënne, W., Van Meirvenne, M., Cornelis, W., 2016. Predicting saturated hydraulic conductivity in a sandy grassland using proximally sensed apparent electrical conductivity. Journal of Applied Geophysics 126, 35–41. https://doi.org/10.1016/j.jappgeo.2016.01.010

Serrano, J., Shahidian, S., da Silva, J.M., 2014. Spatial and temporal patterns of apparent electrical conductivity: DUALEM vs. Veris sensors for monitoring soil properties. Sensors 14, 10024–10041. https://doi.org/10.3390/s140610024

Stermitz, R.J., Nielsen, G.A., Long, D.S., 1999. Testing quality of Soil Survey Geographic (SSURGO) database for precision farming, in: Proceedings of the Fourth International Conference on Precision Agriculture. John Wiley & Sons, Ltd, pp. 319–326. https://doi.org/10.2134/1999.precisionagproc4.c27

Varella, H., Guérif, M., Buis, S., 2010. Global sensitivity analysis measures the quality of parameter estimation: The case of soil parameters and a crop model. Environmental Modelling & Software 25, 310–319. https://doi.org/10.1016/j.envsoft.2009.09.012

Viscarra Rossel, R.A., McKenzie, N.J., Adamchuk, V.I., Sudduth, K.A., Lobsey, C., 2011. Proximal soil sensing. An effective approach for soil measurements in space and time, in: Advances in Agronomy. pp. 237–282.

Yang, J., Wang, J., Xu, C., Liao, X., Tao, H., 2022. Modeling the spatial relationship between rice cadmium and soil properties at a regional scale considering confounding effects and spatial heterogeneity. Chemosphere 287, 132402. https://doi.org/10.1016/j.chemosphere.2021.132402

Zare, S., Abtahi, A., Fallah Shamsi, S.R., Lagacherie, P., 2021. Combining laboratory measurements and proximal soil sensing data in digital soil mapping approaches. CATENA 207, 105702. https://doi.org/10.1016/j.catena.2021.105702